Effect of Post-Weld Heat Treatment on the Fatigue Properties of Dissimilar Titanium Alloy Joints

S.Q. Wang[1, 2], J.H. Liu[2], D.L. Chen[1,*]

[1]Department of Mechanical and Industrial Engineering, Ryerson University, Toronto, Ontario M5B 2K3, Canada
[2]State Key Laboratory of Solidification Processing, Northwestern Polytechnical University, Xi'an 710072, China
* Corresponding author: dchen@ryerson.ca

Abstract The purpose of this study was to characterize the microstructural change and fatigue resistance of electron beam welded (EBWed) dissimilar joints between Ti-6Al-4V and BT9 (Ti-6.5Al-3.5Mo-1.5Zr) alloys after two types of post-weld heat treatment (PWHT), namely only aging and solution treatment followed by aging (STA). It was observed that no significant microstructural change occurred in the FZ after only aging and the high hardness in the fusion zone (FZ) remained, while coarse acicular α occurred in the FZ in the STA condition, leading to a reduced hardness. Both types of post-welded joints were cyclically stable at lower strain amplitudes of 0.2-0.6%, and exhibited cyclic softening at higher strain amplitudes of 0.8%-1.2%. As the total strain amplitude increased, cyclic stress amplitude increased, while the fatigue life decreased. Fatigue crack initiation occurred from the specimen surface or near-surface defects and propagation was characterized mainly by the formation of characteristic fatigue striations.

Keywords Titanium alloy, Post-weld heat treatment, Microstructure evolution, Strain-controlled fatigue.

1. Introduction

Welding is one of the most widely used and economical joining processes for titanium alloys, which makes it possible to create composite structures in the welded joints for various purposes. However, in the electron beam welding (EBW) and laser beam welding, the fusion zones are known to exhibit poor ductility due to the large prior β grain size and a wholly or partially martensitic microstructure [1]. The low thermal conductivity of titanium alloys causes superheating in the heat-affected zone (HAZ), increases the grain size and gives rise to residual stresses in the HAZ, exerting a negative effect [2]. It is necessary to adjust unstable microstructure of the as-welded joints [3]. The post-weld heat treatment (PWHT) is one of the commonly-used methods which could stabilize microstructure, decrease the inhomogeneity of the structure and increase the mechanical properties of the welded joint. Arenas and Acoff [4] reported that PWHT promotes the formation of γ phase in the fusion zone of a gas tungsten arc (GTA) welded gamma titanium aluminide alloy. Guo *et al.* [5] observed that there was no significant hardness increase in fusion zone (FZ) at Ti-64 side of a dissimilar linear friction weld between Ti-64 and Ti-6246 alloys after PWHT. Tuppen *et al.* [6] performed stress-controlled fatigue tests to determine S-N curves of diffusion-bonded dissimilar Ti-6Al-4V/Ti-4Al-4Mo-2Sn-0.5Si titanium alloy joints. Fu *et al*. [7] studied the effects of electron beam local heat treatment (EBLHT) on strain-controlled fatigue properties of EBWed Ti-6Al-4V alloy joints, and their results showed that Ti-6Al-4V alloy joints with and without EBLHT exhibited cyclic softening and the fatigue life of the joints after EBLHT could increase by 30%. Despite the extensive studies on the weldability of titanium alloys, it is unknown if the PWHT would have a significant effect on the microstructure and cyclic deformation behavior of electron beam welds between Ti-6Al-4V and BT9 (Ti-6.5Al-3.5Mo-1.5Zr) alloy. The aim of this study was, therefore, to identify the effect of two common PWHT processes, namely aging with or without solution heat treatment, on the microstructure and fatigue performance of welded joints.

2. Material and Experimental Procedure

The materials used in the present study were forged 10 mm thick Ti-6Al-4V and BT9 titanium

alloys, with the chemical compositions listed in Tables 1 and 2, respectively. Both alloys were machined into the plates of 140 mm × 80 mm × 10 mm, and then mechanically and chemically cleaned before welding. EBW was performed using HDZ-15B EBW machine with an accelerating voltage (V) of 60 kV, an electron beam current (I_b) of 68 mA, an focus current (I_f) of 2230 mA, and a welding speed (v) of 500 mm/min.

Table 1. Chemical composition of Ti-6Al-4V titanium alloy

Element	Al	V	Fe	C	N	H	O	Ti
Content (wt.%)	6	4	0.3	0.1	0.05	0.015	0.2	balance

Table 2. Chemical composition of BT-9 titanium alloy

Element	Al	Mo	Zr	Si	Fe	C	N	H	O	Ti
Content (wt.%)	6.5	3.5	1.5	0.3	0.25	0.1	0.05	0.012	0.15	balance

PWHT was carried out in a vacuum furnace at a vacuum degree of 10^{-2} Pa. One of the welded joints was subjected to solution treatment at a temperature of 950°C for 1 h followed by furnace cooling and then aging at 550°C for 4 h followed by air cooling, and the other joint was directly subjected to aging at a temperature of 550°C for 4 h followed by air cooling. Microstructures were examined (after etching using Keller's reagent) via optical microscopy. Microhardness was determined across the welded joint of mid-thickness (i.e., at a distance of 5 mm from the bottom surface) using a computerized Buehler hardness tester with a load of 500g and a dwell time of 15s at an interval of 0.1 mm.

Fatigue specimens with a gauge length of 12 mm and a width of 3 mm were machined perpendicularly to the welding direction using electro-discharge machining (EDM). The gauge area was ground up to #600 SiC papers to remove the EDM cutting marks and to achieve a smooth surface. Total strain-controlled, pull-push type fatigue tests were conducted in air at room temperature using a computerized Instron 8801 fatigue testing system at different strain amplitudes up to 1.2%. A triangular waveform with a strain ratio of R_s=-1 was applied at a constant strain rate of 1×10^{-2} s^{-1}, where R_s is the ratio of the minimum strain to the maximum strain. The strain-controlled test at low strain amplitudes was continued until 10,000 cycles, after which it was changed to load control at 50 Hz. At least two specimens were tested at each strain amplitude. Fatigue crack initiation site and crack propagation mechanisms were examined on the fracture surfaces of failed samples using SEM.

3. Results and Discussion

3.1 Microstructure

Fig.1(a) and (b) show the microstructure of the two BMs, respectively. It is seen that both Ti-6Al-4V and BT9 had a typical bimodal microstructure, consisting of a combination of equiaxed α grains and inter-granular $\alpha + \beta$ lamellae. However, Ti-6Al-4V contained more equiaxed α grains than BT9. Fig.1(c), (d) and (e) show a significant microstructural changes in the FZ and HAZ after EBW between Ti-6Al-4V and BT9 alloys. The FZ was mainly composed of acicular and fine martensite α' (Fig.1(d) and (e)) due to the rapid cooling during EBW. The HAZ at Ti-6Al-4V side also consisted of acicular martensite α' (Fig.1(e)) but larger in size. The inner-HAZ at BT9 side consisted of a mixture of acicular martensite α', primary α and metastable β (Fig.1(d)), while the outer-HAZ mainly consisted of primary α and metastable β (Fig.1(c)). Fig.2 shows the microstructure of the joints in the aging condition. From these optical images, no significant

difference of microstructures in both FZ and HAZ was observed between the as-welded and the aging conditions, which was in agreement with the previous observations on the electron beam and laser beam welding of Ti-6Al-4V alloy [7,8]. Fig.3 shows the microstructure of the joints in the PWHT condition of solution heat treatment followed by aging (STA). After STA the microstructure of both FZ and HAZ at Ti-6Al-4V side (Fig.3(a)) became coarse α platelets with interlamellar β, which was due to high solution temperature and slow cooling rate, while α platelets, primary α and interlamellar β appeared in the HAZ at BT9 side (Fig.3(b)).

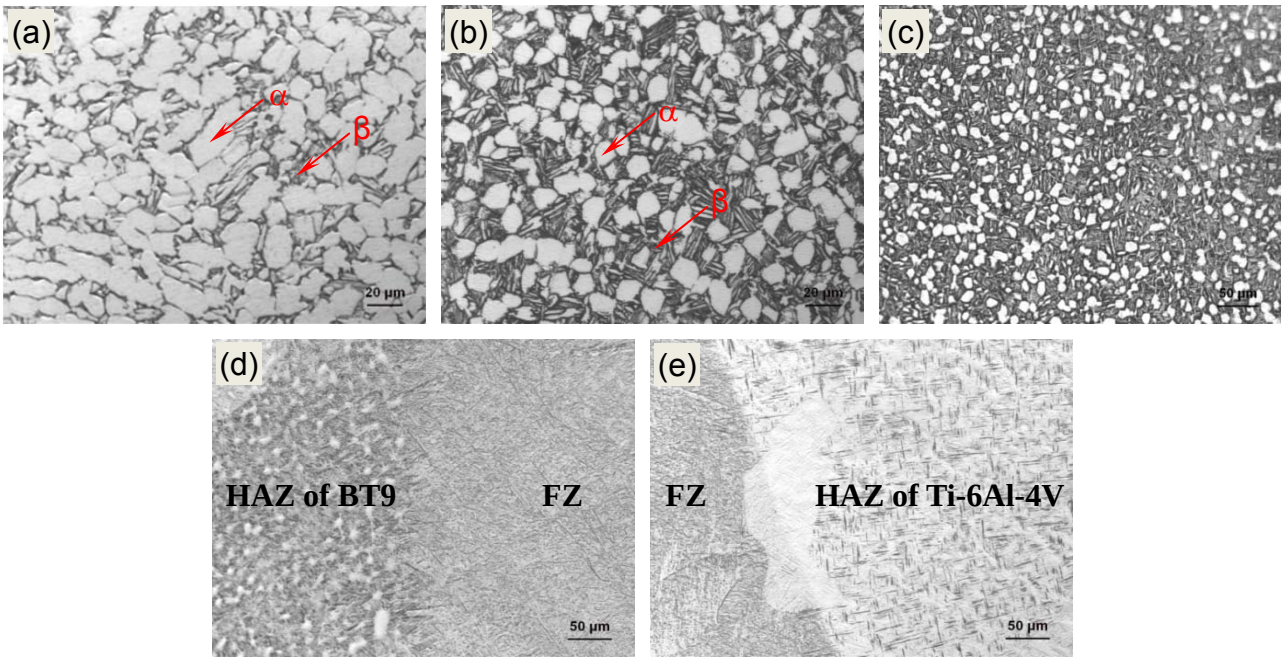

Figure 1. Microstructure of as-welded joint between Ti-6Al-4V and BT9 alloys (a) Ti-6Al-4V BM, (b) BT9 BM, (c) outer-HAZ of BT9, (d) HAZ of BT9 and FZ, and (e) FZ and HAZ of Ti-6Al-4V

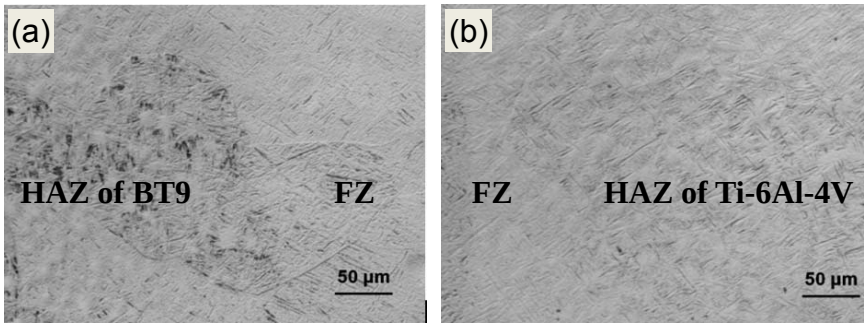

Figure 2. Microstructure of the post-welded joint after aging (a) HAZ of BT9 and FZ, and (b) FZ and HAZ of Ti-6Al-4V

3.2 Microhardness

Vickers microhardness profiles across the dissimilar joint between Ti-6Al-4V and BT9 with and without PWHT are shown in Fig.4. It is seen from Fig.4(a) that an asymmetrical hardness profile across the weld was obtained with an average hardness values of about 300 HV for Ti-6Al-4V BM and approximately 320 HV for BT9 BM, respectively. The higher hardness value in the FZ was due to the formation of martensite in the FZ, as shown in Fig.1(d) and (e). It is observed that the hardness value in the HAZ on the Ti-6Al-4V side was higher than that of the Ti-6Al-4V BM, the hardness value in the inner-HAZ on the BT9 side was also higher than that of the BT9 BM.

However the hardness value in the outer-HAZ was slightly lower than that of the BT9 BM, meaning that a narrow soft zone appeared due to the appearance of β phase as shown in Fig.1(c). The aging treatment at 550°C (Fig.4(a)) led to the elimination of the soft zone at the BT9 side and a slightly higher hardness in the FZ. The increase of hardness was mainly due to the presence of the fine α' and precipitation of some secondary α phase in the β phase both in FZ and HAZ. These results are similar to those reported by Kabir *et al.* [9]. In addition, the microhardness values in the HAZ were also observed to decrease gradually as the distance increased from the FZ border line. This was attributed to the decreasing fine α' and secondary α phase in the HAZ. However, after STA the hardness value in the FZ and HAZ was only slightly higher than or nearly the same as that of the BMs due to the coarse lamellar $\alpha + \beta$ structure (Fig.4(b)). It is of special interest to observe that the narrow soft zone in the outer-HAZ on the BT9 side disappeared as well after STA due to the decomposition of β phase.

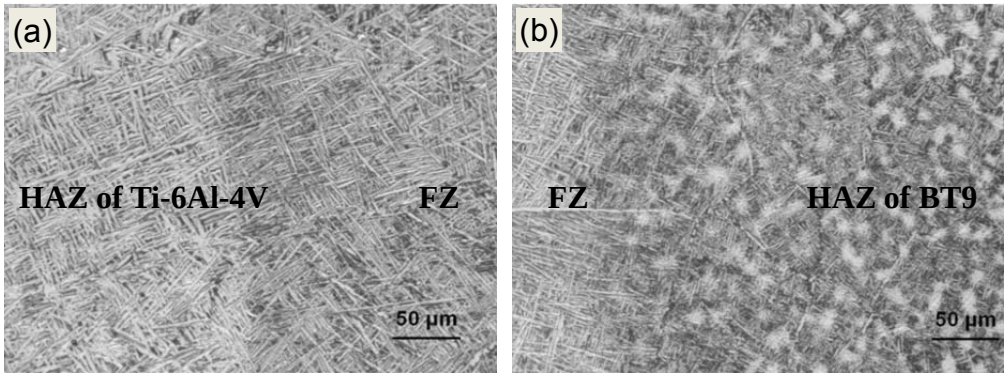

Figure 3. Microstructure of the post-welded joint after STA (a) HAZ of Ti-6Al-4V and FZ, and (b) FZ and HAZ of BT9

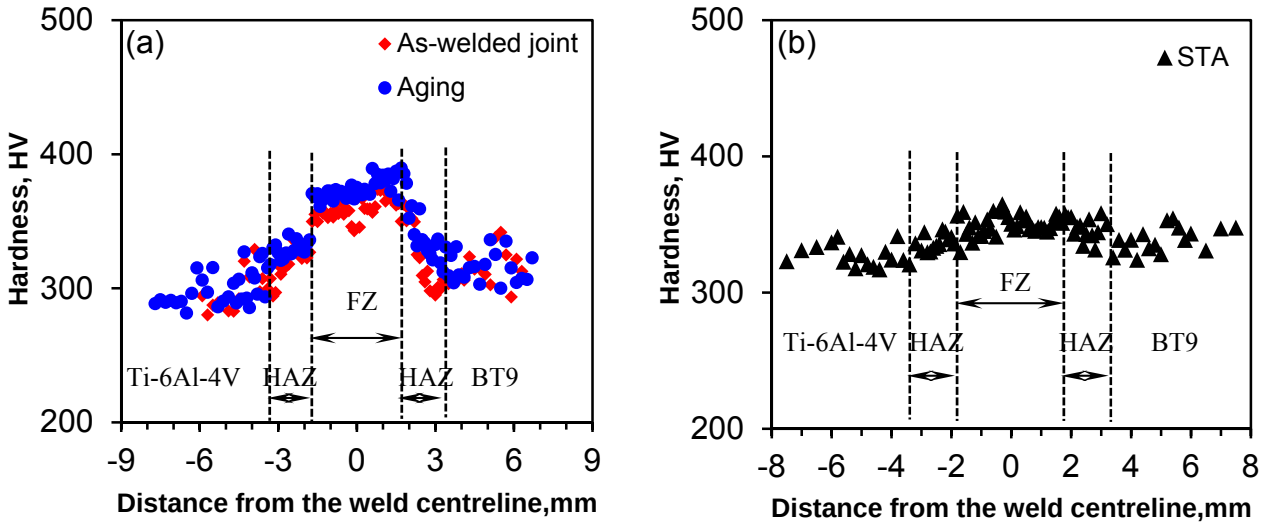

Figure 4. Hardness distribution of the welded joint in (a) as-welded and aging conditions, and (b) STA condition

3.3 Hysteresis loops

The hysteresis loops of the first cycle and mid-life cycle at a total strain amplitude of 1.2% are plotted in Fig 5(a) and (b), respectively. It is seen that the initial tensile (or ascending) phase of the first quarter cycle represented indeed a tensile stress-strain curve tested at a strain rate of 1×10^{-2} s^{-1}. Then the tensile yield strength (YS) of the post-welded joints can be determined from the initial

quarter cycle, and the obtained YS is listed in Table 3. The YS of the post-welded joints in the aging and the STA conditions were almost equal. In addition, the first and mid-life hysteresis loops in both aging and STA conditions were basically symmetrical (Fig.5(a) and (b)). Similar symmetrical hysteresis loops were also observed in titanium alloy [10-13].

3.4 Cyclic deformation response

Figs 6 (a) and (b) show the evolution of cyclic stress amplitude as a function of the number of cycles at different strain amplitudes in the aging and STA conditions, respectively. It is seen that as the applied total strain amplitude increased, cyclic stress amplitude increased and the fatigue life decreased. In both aging and STA conditions, the stress amplitude remained basically constant or stable at the lower strain amplitudes (0.2-0.6%); as the strain amplitude increased (0.8-1.2%) cyclic softening basically occurred, since the post-welded joints lay in a relatively hardened state. Similar cyclic softening characteristics have been documented for titanium alloy under strain-controlled LCF tests [10,14].

Table 3. Fatigue parameters in the aging and STA conditions

Fatigue parameters	σ_y, MPa	n'	K', MPa	σ'_f, MPa	b	ε'_f	c	σ'_y, MPa
Aging	938	0.119	1776	1408	-0.079	0.057	-0.54	865
STA	941	0.116	1759	1412	-0.078	0.109	-0.63	875

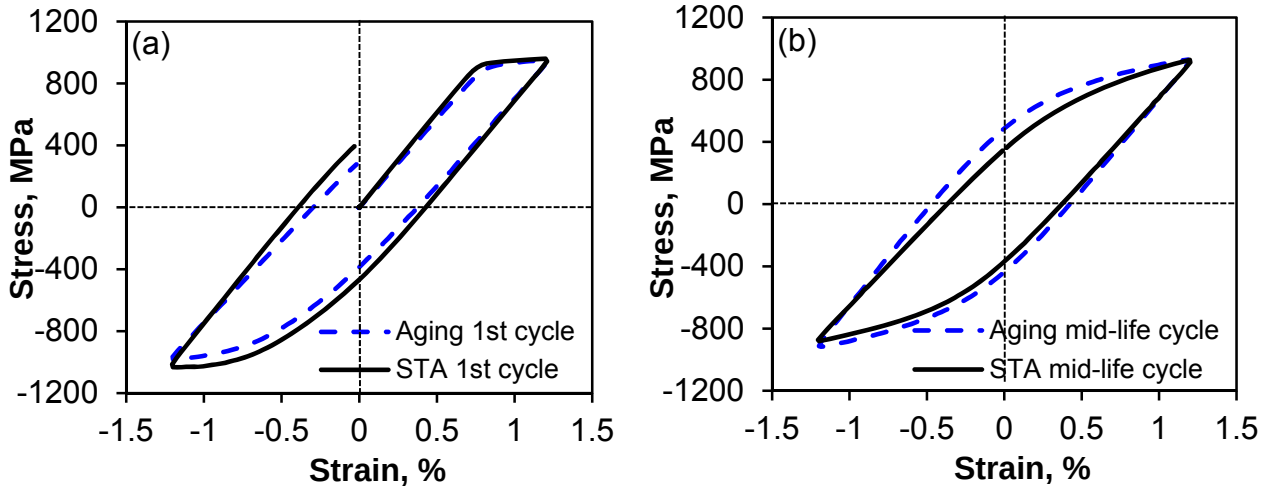

Figure 5. The hysteresis loops at a total strain amplitude of 1.2% and strain ratio of $R_\varepsilon = -1$ for different heat treatment conditions (a) 1st cycle, and (b) the mid-life cycle

Cycling hardening/softening in metals and alloys is known to be dominated by the initial state of the material and the applied strain amplitude. When a material is in its soft/annealed state ($\sigma_{UTS}/\sigma_y \geq 1.4$), cyclic hardening would occur. However, in the hardened state ($\sigma_{UTS}/\sigma_y < 1.2$), cyclic softening would take place [15]. In this study, both types of the post-welded joints exhibited initial cyclic stabilization followed by cyclic softening at the higher strain amplitudes of 0.8-1.2%. The increased degree of cyclic softening with increasing applied strain amplitude might be attributed to the rearrangement and partial annihilation of high density dislocations resulting from EBW [16].

3.5 Fatigue life and fatigue parameters

Fig.7 shows the fatigue lifetime curves of the post-welded joints after aging and STA. Both types of PWHT led to a similar trend of increasing fatigue life with decreasing strain amplitude, and the STA

samples exhibited a slightly lower fatigue life than that of the aging samples at lower strain amplitudes due to the coarser α phase. Based on Basquin equation and Coffin-Manson relation, the total strain amplitude could be expressed as elastic strain amplitude and plastic strain amplitude [15], i.e.,

$$\frac{\Delta\varepsilon_t}{2}=\frac{\Delta\varepsilon_e}{2}+\frac{\Delta\varepsilon_p}{2}=\frac{\sigma'_f\left(2N_f\right)^b}{E}+\varepsilon'_f\left(2N_f\right)^c \quad (1)$$

where E is the Young's modulus, N_f is the fatigue life or number of cycles to failure (the entirety of $2N_f$ is the number of reversals to failure), σ'_f is the fatigue strength coefficient, b is the fatigue strength exponent, ε'_f is the fatigue ductility coefficient, and c is the fatigue ductility exponent. In addition, cyclic deformation behavior is normally considered to be related to the portion of the plastic strain amplitude and is independent of the elastic strain amplitude, which could be expressed by the following equation [15],

$$\frac{\Delta\sigma}{2}=K'\left(\frac{\Delta\varepsilon_p}{2}\right)^{n'}, \quad (2)$$

where $\frac{\Delta\sigma}{2}$ is the mid-life stress amplitude, $\frac{\Delta\varepsilon_p}{2}$ is the mid-life plastic strain amplitude, n' is the cyclic strain-hardening exponent and K' is the cyclic strength coefficient. The obtained fatigue life parameters evaluated on the basis of Equs (1) and (2) were summarized in Table 3. It is also observed that the cyclic strain hardening exponent (n'), the cyclic strength coefficient (K'), fatigue strength coefficient (σ'_f), and cyclic yield strength (σ'_y) of the post-welded joint after aging were nearly the same as that of STA. In general, a smaller absolute value of fatigue strength exponent (b) and fatigue ductility exponent (c) and a larger value of fatigue strength coefficient (σ'_f) and fatigue ductility coefficient (ε'_f) represent a longer fatigue life. This implies that a longer fatigue life of a material in the strain-controlled tests requires a good combination of both high strength and superior ductility. In spite of such a seemingly conflicting effect of the exponent pair (b and c) and the coefficient pair (σ'_f and ε'_f) on the fatigue life, the exponent pair would be expected to play a greater role in the sense of exponential functions. In comparison with STA, the absolute value of c in the aging condition was smaller (while b was nearly the same), and the value of ε'_f was also smaller (while σ'_f remained nearly the same). The combined role of these fatigue life parameters gave no substantial difference between the aging and STA conditions, as also seen in Fig.7. It should be noted that in evaluating the above fatigue life parameters the strain amplitude was limited to a range in-between 0.4% and 1.2%, excluding the strain level with run-out data at which some fatigue samples did not fail at or above 10^7 cycles.

3.6 Fractography

The fracture location of both types of post-welded joints mostly lay in the Ti-6Al-4V BM. Only one sample in the STA condition failed in the HAZ at Ti-6Al-4V side, which might be due to the formation of the coarse α in the HAZ (Fig.3). Fracture surfaces of the fatigued specimens were examined using SEM. Fig.8(a) and Fig.9(a) show an overall view of fracture surfaces of the post-welded joints in the aging and STA conditions at a total strain amplitude of 0.4%, containing regions of fatigue crack initiation, propagation, and final fast fracture. It is seen from these low magnification images that fatigue crack initiated from the specimen surface or near-surface defect, and the river line patterns appeared in both aging and STA conditions which were irregular and

broken and flowed along the crack propagation direction. Fig.8(b)-(c) and Fig.9(b)-(c) show the images near the crack initiation sites and in the crack propagation zone of the fatigued samples at higher magnifications in the aging and STA conditions. In the near-initiation area, a mix of fatigue striations and cleavage-like features could be seen in both aging and STA conditions. Fatigue crack propagation zone was mainly characterized by typical fatigue striations which were perpendicular to the crack propagation direction in both aging and STA conditions.

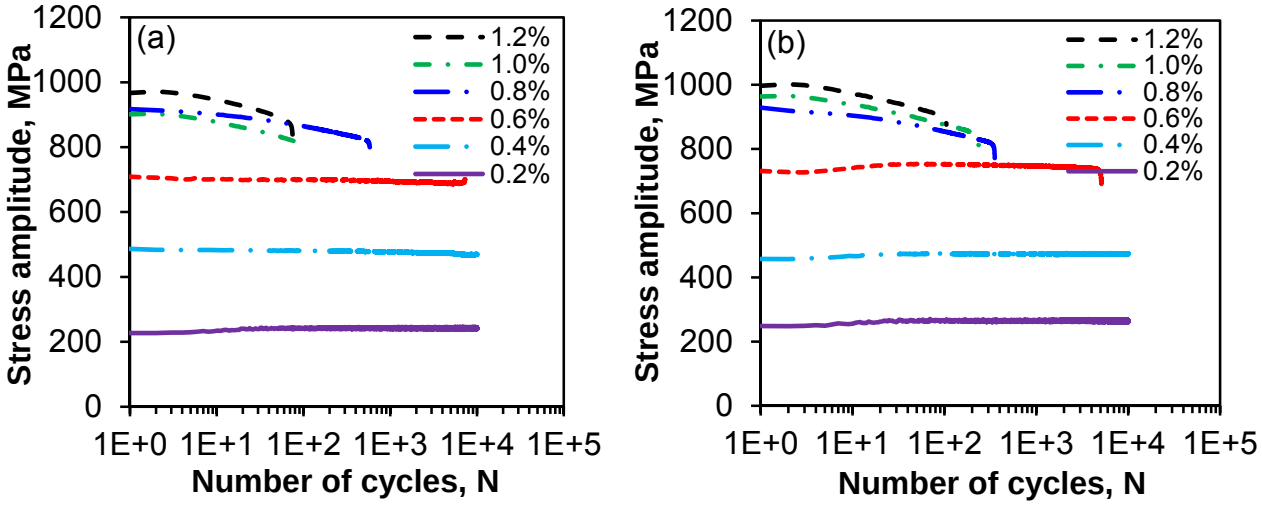

Figure 6. Stress amplitude vs. the number of cycles at different total strain amplitudes in the (a) aging condition, and (b) STA condition

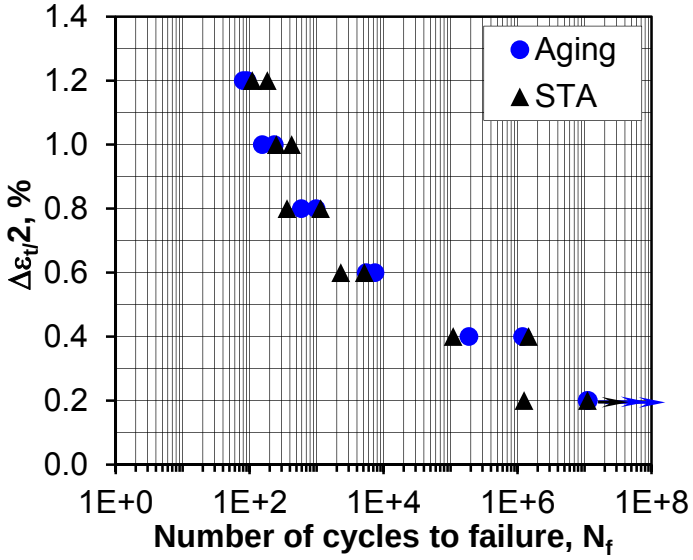

Figure 7. Total strain amplitude as a function of the number of cycles to failure in the aging and STA conditions

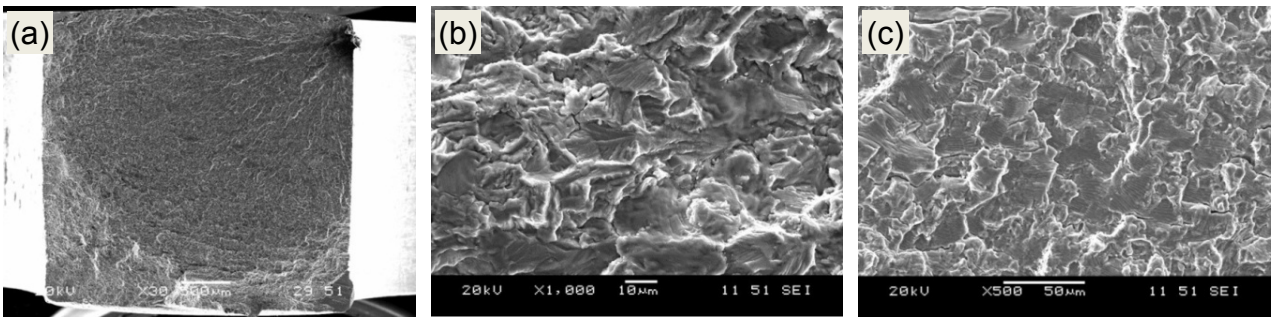

Figure 8. SEM images of fracture surfaces of a post-welded joint in the aging condition, fatigued at a strain

amplitude of 0.4%, (a) an overall view, (b) crack initiation site and (c) crack propagation zone

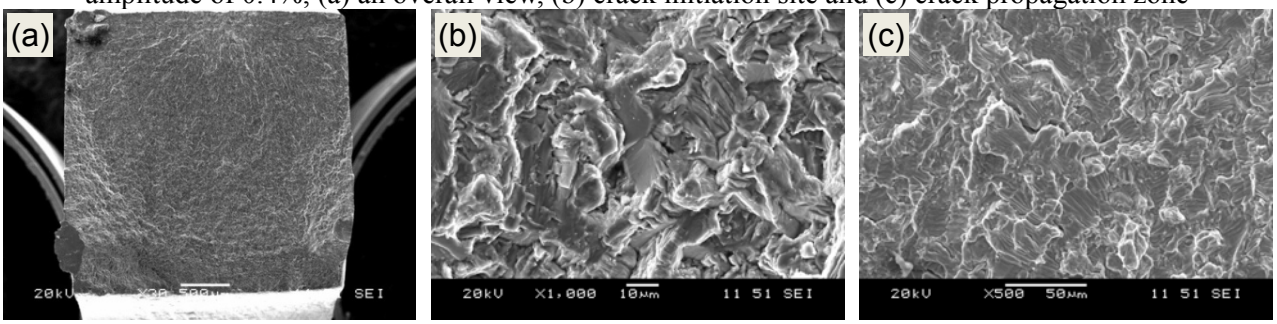

Figure 9. SEM images of fracture surfaces of a post-welded joint in the STA condition, fatigued at a strain amplitude of 0.4%, (a) an overall view, (b) crack initiation site and (c) crack propagation zone

4. Conclusions

1. The microstructure across the dissimilar welded joint exhibited a considerable change, mainly consisting of acicular and fine martensite α' both in the FZ and HAZ of Ti-6Al-4V side, and acicular martensite α', primary α and metastable β in BT9 side, while both BMs of Ti-6Al-4V and BT9 had a microstructure of equiaxed α grains and inter-granular $\alpha + \beta$ lamellae. There was no significant difference in the microstructure of both FZ and HAZ between the as-welded and the aging conditions. However, after STA the microstructure of the FZ and HAZ at Ti-6Al-4V side mainly consisted of coarse α platelets with interlamellar β, while α platelets, primary α and interlamellar β were observed in the HAZ at BT9 side.
2. A characteristic asymmetrical microhardness profile across the dissimilar welded joint was observed with a higher value on the BT9 side than on the Ti-6Al-4V side. The hardness in the FZ was higher than that of both BMs due to the formation of α' martensite arising from the rapid cooling during EBW. A narrow soft zone in the outer-HAZ of BT9 side was observed due to the presence of β phase, while the hardness in the HAZ of Ti-6Al-4V side was higher than that of the Ti-6Al-4V BM. After aging treatment at 550°C the high hardness in FZ remained nearly the same or slightly higher and the narrow soft zone disappeared due to decomposition of β. However, the hardness value of the post-welded joint after STA in both FZ and HAZ was slightly higher than or nearly the same as that of BMs due to the presence of coarsened α.
3. The post-welded joints in both aging and STA conditions displayed cyclic saturation or stabilization in the entire cyclic deformation process at low strain amplitudes up to 0.6%, while cyclic softening occurred after initial cyclic stabilization at higher strain amplitudes. With increasing strain amplitude, the stage of initial cyclic stabilization became gradually shorter.
4. The fatigue life of the aging condition was slightly longer than that of the STA condition at the lower strain amplitudes. In general the strain-controlled fatigue resistance of the post-welded joints in both aging and STA conditions was roughly equivalent.
5. The fatigue fracture of the post-welded joints after aging and STA treatment occurred mostly in Ti-6Al-4V BM. Fatigue crack initiation occurred from the specimen surface or near-surface defect, and crack propagation was mainly characterized by the characteristic fatigue striations coupled with secondary cracks in both aging and STA conditions.

Acknowledgements

The authors would like to thank the Natural Sciences and Engineering Research Council of Canada (NSERC) and AUTO21 Network of Centres of Excellence for the financial support, and

Northwestern Polytechnical University (NWPU), Xi'an, China for providing test materials. One of the authors (D.L. Chen) is also grateful for the financial support by the Premier's Research Excellence Award (PREA), NSERC-Discovery Accelerator Supplement (DAS) Award, Canada Foundation for Innovation (CFI), and Ryerson Research Chair (RRC) program. The authors would also like to thank Messrs. Q. Li, A. Machin, J. Amankrah and R. Churaman for easy access to the laboratory facilities of Ryerson University and their assistance in the experiments.

References

[1] K.K. Murthy, S. Sundaresan, Phase transformations in a welded near α titanium alloy as a function of weld cooling rate and post-weld heat treatment conditions. J Mater Sci, 33 (1998) 817–826.
[2] A.A. Popov, A.G. Illarionov, O.A. Oleneva, Structure and properties of welds of high-alloy titanium alloy after heat treatment. Metal Sci Heat Treat, 52 (2011) 476–480.
[3] G.Q. Wang, Y. Zhao, A.P. Wu, G.S. Zou, J.L. Ren, Microstructure and high-temperature tensile properties of Ti_3Al alloys laser welding joint. Chin J Nonfer Metals, 17 (2007) 1803–1807.
[4] M.F. Arenas, V.L. Acoff, The effect of postweld heat treatment on gas tungsten arc welded gamma titanium aluminide. Scripta Mater, 46 (2002) 241–246.
[5] Y. Guo, Y.L. Chiu, M.M. Attallah, H.Y. Li, S. Bray, P. Bowen, Characterization of dissimilar linear friction welds of α-β titanium alloys. J Mater Eng Perf, 21 (2012) 770–776.
[6] S.J. Tuppen, M.R. Bache, W.E. Voice. A fatigue assessment of dissimilar titanium alloy diffusion bonds. Inter J Fatigue, 27 (2005) 651–658.
[7] P.F. Fu, F.J. Liu, Z.Y. Mao, J.W. Li, Effects of electron beam local heat treatment on fatigue properties for Ti-6Al-4V alloy joints. International Technology and Innovation Conference, Hangzhou, China, November 6-7, 2006, pp. 72–75.
[8] P. Azar, P. Li, P.C. Patnaik, R. Thamburaj, J.-P, Immarigeon, Electron beam weld repair and qualification of titanium fan blades for military gas turbine engine. RTO AVT Specialists' Meeting on "Cost Effective Application of Titanium Alloys in Military Platforms", Loen, Norway, May 7-11, 2001, RTO-MP-069(II), 2001, 18.1–18.16.
[9] A.S.H. Kabir, X.J. Cao, J. Gholipour, P. Wanjara, J. Cuddy, A. Birur, M. Medraj, Effect of postweld heat treatment on microstructure, hardness, and tensile properties of laser-welded Ti-6Al-4V. Metall Mater Trans A, 43 (2012) 4171–4184.
[10] S.J. Li, T.C. Cui, Y.L. Hao, R. Yang, Fatigue properties of a metastable β-type titanium alloy with reversible phase transformation. Acta Biomater, 4 (2008) 305–317.
[11] B. Koch, B. Skrotzki, Strain controlled fatigue testing of the metastable-titanium alloy Ti-6.8Mo-4.5Fe-1.5Al (Timetal LCB). Mater Sci Eng A, 528 (2011) 5999–6005.
[12] Y.H. Lin, K.H. Hu, F.H. Kao, S.H. Wang, J.R. Yang, C.K. Lin, Dynamic strain aging in low cycle fatigue of duplex titanium alloys. Mater Sci Eng A, 528 (2011) 4381–4389.
[13] M. Satoh, S. Horibe, M. Nakamura, H. Uchida, Cyclic deformation and fatigue in TiAl intermetallic compound under plastic strain control. Inter J Fatigue, 32 (2010) 698–702.
[14] J. Plumbridge, M. Stanley, Low cycle fatigue of a titanium 829 alloy. Inter J Fatigue, 4 (1986) 209–216.
[15] E. Dieter, Mechanical Metallurgy, McGraw-Hill, New York, 1986.
[16] A.K. Nag, K.V.U. Praveen, V. Singh, Low cycle fatigue behaviour of Ti-6Al-5Zr-0.5Mo-0.25Si alloy at room temperature. Bull Mater Sci, 29 (2006) 271–275.